Electrostatic Free Energies of Spheres, Cylinders, and Planes in Counterion Condensation Theory with Some Applications

Gerald S. Manning†

Department of Chemistry and Chemical Biology, Rutgers University, 610 Taylor Road, Piscataway, New Jersey 08854-8087

Received July 1, 2007; Revised Manuscript Received August 9, 2007

ABSTRACT: In a previous paper, we have shown that counterions condense on charged spheres and planes as well as on the linear polyelectrolyte models of charged lines and cylinders, provided that the surface charge densities exceed a critical value. Here we give a more complete calculation resulting in the electrostatic free energies of all of these geometric shapes. We consider a macroion immersed in salt solution and also a macroion in the presence only of its own counterions. For a sphere, cylinder, and plane with equal surface charge densities, the sphere has the lowest electrostatic free energy and the plane the highest. We apply the results to the coil-to-globule transition and to the growth of spheres by fusion of two smaller spheres to form a larger one.

I. Introduction

Counterion condensation on linear polyelectrolytes is a well-documented laboratory phenomenon.[1,2] It refers to the adsorption of the counterions into the solvated structure of the polymer such that its net effective charge is reduced to a critical value. If the original fully dissociated bare charge on the polymer is less than the critical value, condensation does not occur. Ultrasonic absorption, index of refraction, and calorimetric signals are direct manifestations of the condensation of counterions,[2] which is also reflected in an electrophoretic mobility that is independent,[3−6] or nearly so,[7] of the amount of charge placed on a polymer of fixed length once a critical charge load has been reached. Because the condensed counterions are intimately involved with the solvated structure of the polymer, the number of condensed counterions and hence the effective charge of the polymer are invariant to salt concentration over a wide range (for example, excess ultrasonic absorption is insensitive to added salt[8]).

The force exerted on a single DNA molecule by an applied electric field has recently been measured in an optical tweezers experiment.[9] The data indicate that the electric field detects an effective DNA charge much less than the bare charge −2 per base pair (two phosphates per base pair). The measured effective charge is -0.50 ± 0.05 per base pair, equivalent to a reduction of the bare charge by $75 \pm 3\%$. The reduction predicted by counterion condensation theory is 76%.[10,11] The DNA effective charge was observed to be independent of salt concentration from 0.02 to 1 M KCl. A control measurement at a single salt concentration found no difference if NaCl was used (this result does not rule out the possibility that condensed Na^+ and condensed K^+ are distributed differently within the solvated DNA structure, for example, some Na^+ ions could penetrate more deeply into the DNA grooves than do K^+ ions[12]).

The documentation of counterion condensation on linear polyelectrolytes extends to theoretical understanding and computational detail.[10−31] Condensation results from the competition of an unfavorable loss of entropy when counterions associate to the polymer and a favorable loss of electrostatic energy when the polymer charge is reduced by the associated counterion charge. The overall effect differs from other association/dissociation systems because in a linear geometry the electrostatic potential of the polymer has a logarithmic dependence on distance, and hence on counterion concentration, and competes on the same footing with the concentration dependence of the dissociation entropy.[10,11] In our hands, the experimentally observed invariance to salt concentration is confirmed by theory. To the extent that some models appear to yield an unrealistic salt dependence, it may be because they do not fully capture the extent of involvement of the condensed counterions with the solvated polymer structure.

The theory of counterion condensation has been used as the basis for a free energy calculation, resulting in a formula that incorporates explicit evaluation of the partition function of the condensed counterions.[10,11] The calculation is nonlinear (as it must be since linear electrostatics does not generate ion condensation), but the part of the free energy that represents the interaction of the effective charge with the uncondensed ions is handled by linear Debye−Hückel electrostatics. This procedure is correct.[27,32] (For verification in simulations, see also Figure 11 of ref 2 and Figure 3 of ref 33.) Many useful applications ensued from the free energy formula.[10,11,34−37]

Somewhat surprisingly, but quite clearly, electrophoretic mobility measurements have exhibited behavior indicative of counterion condensation on spherical macroions.[38−42] The mobility of a charged spherical macroion looks very much like that of a charged linear polymer. A plot of mobility vs surface charge density exhibits a plateau, as though a threshold value of the charge density initiates counterion collapse on the surface, maintaining a constant net value of macroion charge and hence mobility. Perhaps this observation is not so surprising, given that simulations of ionic interactions with planar charged membranes show penetration of counterions inside the charged groups on the membrane surface[43] and given the correlated interfacial hydration and ion-specific effects seen in chemical trapping data for macroions of various morphologies.[44] In any event, the question of effective charges on spheres and planes, as well as on cylindrical models of polyelectrolytes, that are reduced from the bare surface charges by association of counterions has long been the subject of theoretical investigations.[27,45−49]

In a recent paper, we showed that the standard theory of counterion condensation on a polyelectrolyte modeled as either an extended assembly of discrete charges or as a uniformly

† E-mail: jerrymanning@rcn.com.

10.1021/ma071457x CCC: $37.00
Published on Web 09/29/2007

surface-charged thin cylinder could be extended to uniformly surface-charged spheres, thick cylinders, and planes.[50] In all cases, counterions condense on a supercritical bare surface charge, reducing the net charge to the critical value. The difference is that for these macroionic shapes the critical bare surface charge density depends on concentration, whereas the critical condition for the polyelectrolyte model does not.

In this paper, we extend the counterion condensation theory to the calculation of the electrostatic free energy of charged spheres, cylinders, and planes and give some applications. In a first application, we compare the free energies of spheres, cylinders, and planes, all with the same bare surface charge density, so that differences are caused solely by geometrical shape. The subsequent applications are inspired by the extensive investigations of Khokhlov, Khalatur, and their colleagues of linear copolymers designed on the computer and in the laboratory to be "proteinlike", in that they collapse in appropriate conditions to quasi-spherical globules with hydrophilic monomers exposed to solvent and hydrophobic monomers in the interior.[51] The single-chain globules are resistant to large-scale aggregation, even in poor solvent conditions. We are able to model the single-chain coil-to-globule transition and the disintegration of a two-chain globule to two single-chain globules at high temperature. Additionally, we perform a calculation that, while not directly comparable to the simulations, may add to our knowledge of why microaggregates do not necessarily lead to macroscopic aggregation.[51−54]

II. Free Energy Analysis of Charged Spheres, Cylinders, and Planes

A. A Single Macroion Immersed in Salt Solution. We begin our analysis as in our previous paper[50] by listing (with slight change of nomenclature) the Debye−Hückel free energies G^{DH} required to charge an impenetrable sphere of radius a, an impenetrable cylinder of radius a, and a planar wall. The sphere and cylinder are immersed in an infinite solution of bulk simple electrolyte characterized by inverse Debye screening length κ. The wall is bathed on only one side by the electrolyte solution. The charging free energies represent the work required to charge these structures up to their *net* surface charge densities after possible counterion condensation. The *bare* surface charge density before counterion condensation is designated by σ. The counterions have unsigned valence z and are the same as one of the ion species in the simple electrolyte. The free energies ascribe any departure from linear Debye−Hückel electrostatics to collapse of counterions from the diffuse ion atmosphere onto the surface of the macroion, effectively reducing, or "renormalizing", the bare surface charge density. This eventuality is represented by inclusion of a factor $(1 - z\theta)^2$, where θ is the number of counterions per bare unit surface charge collapsed, or condensed, on the macroion. In fact, the Mayer virial expansion indicates that for sufficiently dilute electrolyte, the Debye−Hückel free energy becomes a good approximation *unless* the expansion diverges because of physical ion collapse.[32] See the Introduction for additional references.

The product $z\theta$ could be zero if it turns out on free energy minimization that no counterions are condensed. In any event, it cannot exceed unity, since our formalism is too simple for consideration of charge reversal. The total number of condensed counterions is $N\theta$ if the covalent structure of the macroion includes N unit charges e on its surface. Also appearing in the expressions for the free energies is the Bjerrum length $\lambda_B = e^2/Dk_BT$ (esu/cgs units), where the denominator is the product of dimensionless dielectric constant D of the pure solvent, Boltzmann constant, and absolute temperature. In eq 3 below for the cylinder, the functions $K_0(x)$ and $K_1(x)$ are modified Bessel functions of the second kind. Finally, the cylinder and plane are infinite; the finite number N of unit charges on each of them cancels in the subsequent calculation (or, alternatively, it may be regarded as counting the charge in central sections large enough to overwhelm edge effects).

With this discussion, the free energies of sphere, cylinder, and planar wall are obtained by applying a standard charging procedure to the respective solutions of the Debye−Hückel linearization of the Poisson−Boltzmann equation in the appropriate coordinate systems[55]

$$G^{DH} = 2\pi N k_B T(1 - z\theta)^2(\lambda_B a\sigma/e)f(\kappa a) \tag{1}$$

where for the sphere

$$f(\kappa a) = \frac{1}{1 + \kappa a} \tag{2}$$

and for the cylinder

$$f(\kappa a) = \frac{K_0(\kappa a)}{\kappa a K_1(\kappa a)} \tag{3}$$

and for the planar wall

$$f(\kappa a) = \frac{1}{\kappa a} \tag{4}$$

Notice that for the planar wall there is no radius a, and indeed this quantity cancels from eqs 1 and 4. Further, for a charged plane with electrolyte bathing both sides, $f(\kappa a)$ is half the value given in eq 4.

The Debye−Hückel interactions of the renormalized macroion charge with uncondensed small ions as measured by G^{DH} are not the only contribution to the electrostatic free energy G^{el}. There is also an entropic contribution. The $N\theta$ condensed counterions are transferred to the macroion surface from bulk solution, where their translational entropy was $-N\theta k_B \ln \nu c$, where c is the bulk salt concentration, and ν is the number of counterions in the formula for the salt (so that νc is the counterion concentration). Taking into account as well the free energy of the $N\theta$ counterions when they are condensed, we can write for the transfer free energy

$$G^{transfer} = N k_B T\theta \ln \frac{1000\theta}{\gamma \nu c Q} \tag{5}$$

where γ is an activity coefficient for the counterions in solution, and the salt concentration c is in units of molarity. The local activity of condensed counterions is θ/Q, where Q is an internal partition function for the condensed counterions with units cm^3/(mol macroion charge). We will assume that Q does not depend on θ, which means that we neglect short-range interactions among the condensed counterions, such as the volume they exclude to each other.

It is worth pointing out here that although we will ultimately obtain the overall electrostatic free energy G^{el} as the sum $G^{DH} + G^{transfer}$, the two components are additive only in a highly restrictive sense. The reason is that the number of condensed counterions θ appearing in G^{DH} depends on $G^{transfer}$, and the condensed layer partition function Q that appears in $G^{transfer}$ depends on G^{DH}. The two components are coupled in a nonlinear way by the minimization analysis that we proceed to describe.

The Debye−Hückel interactions and the transfer of counterions from bulk solution to macroion surface are coupled but are nonetheless physically distinct effects, and they are competitive. The former is at a minimum when all counterions are condensed on the macroion surface, neutralizing all of the surface charge and thus eliminating all electrostatic repulsion. The transfer component, on the other hand, is at a minimum when there are no condensed counterions, since then all of the counterions participate in the maximum entropy obtained when they are dissociated from the macroion into bulk solution. To see if a minimum overall free energy can be determined for some intermediate counterion condensation between zero and complete charge neutralization, we can differentiate each of the two components with respect to θ and require that the one derivative equal the negative of the other

$$4\pi z(1 - z\theta)(\lambda_B a\sigma/e)f(\kappa a) = -\ln c + \ln(1000\theta/\gamma\nu Q) + 1 \quad (6)$$

In writing the equilibrium condition eq 6, we have intentionally isolated the ln c term on the right-hand side, which represents the entropy of free counterions and dominates this side of the equation as c is continuously taken toward zero. It is clear that, then, there is no chance for an equilibrated fractional number of condensed counterions, unless the macroion charge density σ on the left-hand side is continuously adjusted to remove the divergence to infinity from the equation. Since the inverse Debye length κ scales like the square root of c, the removal of the divergence can be implemented by requiring the adjustment of σ to be such that the left-hand side is maintained equal to $-2\ln(\kappa\ell)$, where ℓ is some length suitably chosen such that $\kappa\ell$ is a small quantity (in all formulas that follow, it is understood that $-\ln(\kappa\ell)$ is a positive quantity)

$$2\pi z(1 - z\theta)(\lambda_B a\sigma/e)f(\kappa a) = -\ln(\kappa\ell) \quad (7)$$

or

$$1 - z\theta = \frac{e(-\ln \kappa\ell)}{2\pi z\lambda_B a\sigma f(\kappa a)} \quad (8)$$

From this equation it is clear that $1 - z\theta$, the fractional amount of charge on the macroion remaining after counterion condensation, is less than unity if the bare surface charge density exceeds a critical value (equal to the factor multiplying $1/\sigma$ in the preceding equation)

$$\sigma_{crit} = \frac{e(-\ln \kappa\ell)}{2\pi z\lambda_B a f(\kappa a)} \quad (9)$$

Then

$$1 - z\theta = \sigma_{crit}/\sigma \quad (10)$$

For convenience we introduce a reduced charge density $\sigma' = \sigma/\sigma_{crit}$, so that the fractional amount of charge neutralized by condensed counterions is given by

$$z\theta = (\sigma' - 1)/\sigma' \quad (11)$$

Also, since the effective number of charges N_{eff} remaining on the macroion after counterion condensation equals $1 - z\theta$ times the bare number of charges N

$$N_{eff}/N = 1/\sigma' \quad (12)$$

At this point, we know the equilibrium value of θ, and if we return to the full equilibrium condition, eq 6, we can solve it to obtain a self-consistent formula for the internal partition function Q of the condensed layer of counterions

$$Q = 4\pi\mathbf{e}N_{Av}[(\nu + \bar{\nu})/\gamma\nu]\bar{z}\lambda_B\ell^2(\sigma' - 1)/\sigma' \quad (13)$$

where N_{Av} is Avogadro's number, $\mathbf{e}$ is the base of natural logarithms, and $\bar{\nu}$ and $\bar{z}$ are, respectively, the number of co-ions in the formula for the salt and the unsigned valence of the co-ion. In generating this formula, we used the complete expression for the square of the Debye parameter in a solvent containing a single salt of molarity c

$$\kappa^2 = (8\pi) \times 10^{-3}N_{Av}\lambda_B I \quad (14)$$

where I, the ionic strength, is defined by $(1/2)(\nu z^2 + \bar{\nu}\bar{z}^2)c$, and may be written in the form $(1/2)(\nu + \bar{\nu})z\bar{z}c$.

With eq 11 for θ, the fraction of counterions condensed, and eq 13 for the internal partition function Q, we can work out a formula for G^{el}, the overall electrostatic free energy of the macroion, by summing G^{DH} from eq 1 and $G^{transfer}$ from eq 5. After some calculation we arrive at a result with simple appearance

$$\frac{zG^{el}}{Nk_BT} = -\left(2 - \frac{1}{\sigma'}\right)\ln(\kappa\ell) - 1 + \frac{1}{\sigma'} \quad (15)$$

Notice that the activity coefficient γ has canceled out, and notice especially that the electrostatic free energy is a positive quantity, since $\kappa\ell$ is small.

Everything we have written thus far pertains to a macroion with charge density greater than critical, $\sigma' > 1$, but it is also worth specifying the electrostatic free energy for the case $\sigma' < 1$. For these subcritical charge densities, there are no condensed counterions, and the electrostatic free energy is simply the Debye−Hückel work required to charge the macroion as given by eq 1 with $\theta = 0$. It is easy to show that it may be written in the form

$$zG^{el}/Nk_BT = -\sigma'\ln(\kappa\ell) \quad (16)$$

Notice that in this range, the free energy is linear in the charge density, as must be true of a purely Debye−Hückel model. Notice the contrast with the decidedly nonlinear form of the free energy for supercritical charge densities, eq 15, which goes well beyond Debye−Hückel by incorporating condensed counterions and their internal free energy into the model. Finally, notice that the subcritical and supercritical electrostatic free energies are continuous at the critical point, $\sigma = \sigma_{crit}$, $\sigma' = 1$.

In our general treatment there has been no need to distinguish among spheres, cylinders, and planes. For the free energy involved in a given application, however, the macroion geometry must be specified in order to determine the reduced surface charge density σ' and the scaling length ℓ in the small quantity $\kappa\ell$, both of which enter into the expression for G^{el} in either its subcritical form eq 16 or its supercritical form eq 15. In turn, the function $f(\kappa a)$ needed to compute σ' from eq 9 is different for the different geometries.

We have previously defined a small sphere as one with radius a much less than the Debye screening length.[50] Then, $\kappa a \ll 1$ serves as our small quantity and also may be neglected in eq 2. For the *small sphere*

$$\ell = a, f(\kappa a) = 1 \quad (17)$$

Similarly, a thin cylinder of radius a is a cylinder in solution conditions such that $\kappa a \ll 1$, so that the asymptotically limiting form of eq 3 may be used. For the *thin cylinder*

$$\ell = a,\ f(\kappa a) = -\ln \kappa a \tag{18}$$

A large sphere has a radius a comparable to or larger than the Debye length, so that κa is not small. For it, ℓ is the Bjerrum length, and the full eq 2 is used. For the *large sphere*

$$\ell = \lambda_B,\ f(\kappa a) = \frac{1}{1+\kappa a} \tag{19}$$

The quantity κa is again not small for a thick cylinder of radius a, and the full eq 3 is used. For a *thick cylinder*

$$\ell = \lambda_B,\ f(\kappa a) = \frac{K_0(\kappa a)}{\kappa a K_1(\kappa a)} \tag{20}$$

Finally, for a *plane wall* of infinite radius a (which cancels in all formulas involving it, creating no difficulties)

$$\ell = \lambda_B,\ f(\kappa a) = \frac{1}{\kappa a} \tag{21}$$

The case of the thin cylinder requires some discussion. The uniform surface charge density σ for a cylinder of radius a may be written as $e/(2\pi ab)$, where b is the length of a cylindrical segment that contains one elementary charge e. But from eq 9 for the case of a *thin* cylinder, $\sigma_{crit} = e/(2\pi z \lambda_B a)$. The ratio of these two quantities is σ', and for the thin cylinder, therefore, $\sigma' = z\xi$, where $\xi = \lambda_B/b$ is the familiar polyelectrolyte charge spacing parameter.[1,11] Therefore, the threshold conditions for counterion condensation on an open polyelectrolyte chain, $z\xi > 1$, and on a thin cylinder, $\sigma' > 1$, are identical.

The electrostatic free energy of a thin cylinder is given either by eq 15 if $\sigma' < 1$ or by eq 16 if $\sigma' > 1$, along with eq 18. These formulas are identical to the corresponding polyelectrolyte formulas based on the model of a line of discrete point charges with spacing b in the limiting conditions $\kappa b \ll 1$,[11] except that $\ln(\kappa a)$ in the former is replaced by $\ln(\kappa b)$ in the latter. The difference is significant. It means that the thin cylinder model gives a divergent free energy as the radius tends to zero, while the line of discrete charges does not possess this pathological behavior.

B. A Macroion in the Presence Only of Its Own Counterions. In the applications, we shall dwell on computer simulations in which no added salt is present.[51] The macroions are exposed only to solvent and a neutralizing number of counterions. For the present theory, we then have to recognize that the Debye screening parameter κ depends on the number of condensed counterions, since it is set only by the counterions in free solution

$$\kappa^2 = (4\pi) \times 10^{-3} N_{Av} \lambda_B z(1 - z\theta)c \tag{22}$$

where here $N_{Av}c$ is the number density of bare macroion charges, that is, the ratio of N to solution volume (in cm^3), so that $N_{Av}[(1 - z\theta)/z]c$ is the number density of uncondensed counterions. If we differentiate both sides of this equation by θ, we get

$$\partial\kappa/\partial\theta = -(1/2)[z/(1 - z\theta)]\kappa \tag{23}$$

A function $f(\kappa a)$ appears in the Debye−Hückel free energy component as given by eq 1. Here we need its derivative with respect to θ

$$\partial f(\kappa a)/\partial\theta = -(1/2)\kappa a f'(\kappa a)[z/(1 - z\theta)] \tag{24}$$

where $f'(\kappa a)$ is the derivative of $f(\kappa a)$ with respect to κa. With this preparation, it is easy to show that the θ derivative of the free energy component G^{DH} is the same as in the case of the salt solution, with the exception that the function $f(\kappa a)$ is replaced by a corrected function $\phi(\kappa_0 a)$

$$\phi(\kappa_0 a) = f(\kappa_0 a)\left[1 + \frac{1}{4}\kappa_0 a \frac{f'(\kappa_0 a)}{f(\kappa_0 a)}\right] \tag{25}$$

For the change of notation from κ to κ_0, see the discussion below along with eq 26. We note also that according to eq 25, ϕ and f are asymptotically equal for small values of their arguments for the case of the thin cylinder, an equality implying identical threshold conditions for counterion condensation on a thin cylinder and on a line-of-charges model.

Turning to the free energy of transferring $N\theta$ counterions from their completely dissociated state at concentration c/z to the macroion surface, we can remark that it is given again by eq 5 if ν is replaced by z^{-1}. Its θ derivative is therefore unchanged, except for this replacement.

We now follow the procedure for the case of the salt solution, but we have to hesitate as soon as the left-hand side of the equilibrium equation is set equal to $-\ln(\kappa\ell)$, as in eq 7. The problem is that κ now depends on θ, and we cannot solve straightforwardly for θ as we did in obtaining eq 11. We circumvent this difficulty with a first-order perturbation procedure. We start with $\theta = 0$, so that κ becomes based on the total concentration of counterions c/z

$$\kappa_0^2 = (4\pi) \times 10^{-3} N_{Av} \lambda_B z c \tag{26}$$

Then we can get a first-order solution for θ by continuing to follow the procedure for salt solutions. Everything goes through with no further difficulty, and we state the results.

The fraction $z\theta$ of macroion charge neutralized by condensed counterions is given by eq 11, where $\sigma' = \sigma/\sigma_{crit}$, and σ_{crit} is given by eq 9 with κ replaced by κ_0 and $f(\kappa a)$ replaced by $\phi(\kappa_0 a)$. The internal partition function Q of the condensed layer is given by the equation

$$Q = 4\pi \mathbf{e} N_{Av} \gamma^{-1} \lambda_B \ell^2 z^2 (\sigma' - 1)/\sigma' \tag{27}$$

The total electrostatic free energy of the macroion is given by eq 15 with κ replaced by κ_0. The effective number of charges on the macroion after counterion condensation is given by eq 12. All of these statements are valid in the supercritical range of surface macroion charge densities $\sigma' > 1$. The results for the subcritical range are exactly the same as in the case of salt solutions, except that the Debye screening parameter κ is given by eq 26 (with no approximation involved, since θ is indeed equal to zero for subcritical charge densities). Finally, in both subcritical and supercritical charge density ranges, the length ℓ is the same as for the case of salt solutions; ℓ is the radius of a small sphere or thin cylinder, and it equals the Bjerrum length for a large sphere, a thick cylinder, or a plane wall.

III. Ranking of Spheres, Cylinders, and Planes

As a first application of the foregoing results, we can rank spheres, cylinders, and plane walls according to their electrostatic free energy; in other words, according to the amount of work required to establish their electrical charge. We restrict the comparison to surfaces with the same bare charge densities σ. Then any differences in the electrostatic free energies per

unit surface area must be ascribed solely to geometical differences in the surface curvatures.

We begin in the subcritical range of Debye−Hückel free energies, where it is easy to work directly from eqs 1−4 with $\theta = 0$. For example, let g_{sphere}/g_{cyl} be the ratio of electrostatic free energies per bare surface charge of a sphere and a cylinder with the same radius a and the same surface charge density σ. Since the charge densities are the same, this ratio is the same as the ratio of free energies per unit surface area. This ratio is then given by the corresponding ratio of $f(\kappa a)$ functions from eqs 2 and 3. With the aid of numerical plots, it becomes clear that $g_{sphere} < g_{cyl}$. Similarly, we find that $g_{cyl} < g_{plane}$, where g_{plane} is the electrostatic free energy per unit surface area of a plane wall with the same surface charge density as the cylinder. We conclude that in the subcritical range of charge densities the electrostatic "tension" per unit surface area in a sphere and a cylinder of the same radius, and a plane wall, all with the same surface charge densities, increases in the order sphere < cylinder < plane wall. This result is independent of whether the solution contains excess salt or only the ions countering the surface charge.

The comparison in the supercritical range is more delicate. We assume at the outset that the common surface charge density σ for all of the shapes exceeds all of the critical charge densities for these shapes. We can begin by multiplying eq 15 through by the common charge density σ. Then, on the left stands a positive constant times the electrostatic free energy per unit surface area, while on the right is the product of σ and a function of σ'. If we now differentiate the right-hand side with respect to σ', keeping σ and the length ℓ fixed, we find that the derivative is always positive, provided that $\kappa\ell$ is a small quantity, as it must be for validity of the formula. Since $\sigma' = \sigma/\sigma_{crit}$, this observation means that the free energy per unit surface area is inversely correlated with the critical charge density; it increases if the critical charge density decreases (at fixed values of σ and ℓ).

We pause to indicate why this particular result makes some sense. The meaning of a decreasing critical charge density is that the surface starts condensing counterions at lower charge density thresholds. Counterions condense to relieve electrostatic stress. So the surface with lower condensation threshold has the higher electrostatic stress.

It remains to compare critical charge densities for sphere, cylinder, and plane wall. Since ℓ must be fixed, we can compare in the first instance a small sphere to a thin cylinder of common radius a, since $\ell = a$ for both (see preceding section). We recall the definitions from the preceding section of a small sphere and thin cylinder as objects with radial dimension much smaller than the radius of the Debye screening atmosphere, $\kappa a \ll 1$. For these geometries, we obtain the respective critical charge densities from eq 9 with $\ell = a$ and the respective functions $f(\kappa a)$ as indicated in the preceding section. It then becomes obvious that the critical charge density of a small sphere is greater than the critical charge density of a thin cylinder with the same radius. Therefore, the electrostatic free energy per unit surface area of a thin cylinder is greater than that of a small sphere, even though the two objects have equal bare charge densities σ.

We can also compare the plane wall with a thick cylinder and a large sphere, since ℓ has the common value of the Bjerrum length λ_B for all three shapes (see previous section). Again, we recall from the previous section the definitions of "thick" and "large" as implying a radial dimension comparable to or larger than the width of the Debye atmosphere, which then forms a thin layer around the sphere or cylinder (but still more diffuse than the layer of condensed counterions). The critical charge densities are obtained from eq 9 with $\ell = \lambda_B$ and $f(\kappa a)$ as indicated in the prescriptions of the preceding section. These critical charge densities decrease from large sphere to thick cylinder to plane wall. Therefore, the electrostatic free energies per unit surface area are all different for these objects, even though their surface charge densities σ may be the same. The large sphere has the smallest of the surface free energy densities, the plane wall the largest, while a thick cylinder (of the same radius as the sphere) has an intermediate value. We give a numerical example in Figure 1, where the free energy per unit surface area of a large sphere is compared with that of a plane wall with the same surface charge density as the sphere.

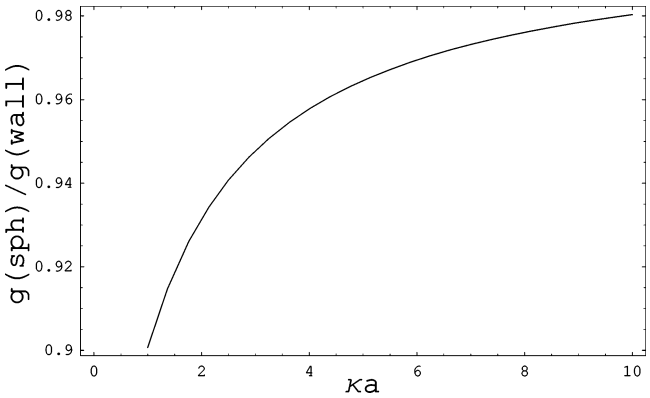

Figure 1. Plot of the ratio of electrostatic free energies per unit surface area of a large sphere and a plane wall in the supercritical range. For this case, the ratio of critical charge densities (sphere *to* plane) is $(1 + \kappa a)/\kappa a$, where a is the sphere radius. As numerical values, we choose 0.1 for the small quantity $\kappa\lambda_B$, and 2 for σ' of the large sphere. Then σ' for the plane wall equals $2(1 + \kappa a)/\kappa a$. The plot shows that the electrostatic free energy per unit surface area of the sphere is smaller than of the plane wall, even though sphere and wall have equal bare surface charge densities.

The above results were computed for the excess salt case. If the only small ions present are the counterions of the macroion, then the prescription of the preceding section leads to the same result for a small sphere and a thin cylinder of the same radius and surface charge density; the free energy per unit surface area is greater for the cylinder. Further, the same ordering is found for the large sphere, the thick cylinder with the same radius as the sphere, and the plane wall, all with the same supercritical surface charge densities; the ordering of electrostatic free energies per unit surface areas is sphere < cylinder < plane wall.

IV. Coil-to-Globule Temperature Transition

In 1998, Khokhlov and Khalatur initiated a series of polymer-design papers marked by exceptional ingenuity.[51] They designed, on the computer, a "proteinlike" copolymer in such a way that the polymer collapses to a globule with hydrophobic groups in the core and hydrophilic groups on the solvent-exposed surface. Both laboratory and computer experiments have been performed to gain a detailed understanding of the properties of these polymers, which in some ways are able to mimic biological behavior.

In a brief description of the design of the copolymers, interactions between monomers in an initial homopolymer are set to a uniform attraction. The polymer is then observed to form a dense globule. Monomers on the surface of the globule are labeled $\mathscr{P}$ (polar, or hydrophilic), and those in the interior are labeled $\mathscr{H}$ (hydrophobic). The attractive interactions are then turned off, and the $\mathscr{HP}$ copolymer becomes a random coil. If

$\mathscr{H}\mathscr{H}$ interactions are then reset to be attractive, a compact morphology is observed at low temperature with $\mathscr{H}$ monomers mainly in the interior and $\mathscr{P}$ monomers exposed to the solvent. In a biological context, the proteinlike behavior is the ability of this primary sequence of $\mathscr{H}$ and $\mathscr{P}$ "amino acids" to fold into a tertiary "native" structure. By several measures, the folding is more efficient than with copolymer sequences engineered in more obvious ways.

Khalatur et al.[56] and Mologin et al.[57] reported molecular dynamics simulations on a class of these copolymers in which the hydrophilic groups $\mathscr{P}$ each bore a negative charge. The authors studied the behavior of the charged copolymers in interaction with univalent, divalent, and tetravalent counterions. Although the characteristics of this system are expected to depend quantitatively on the specially designed sequence of charged and neutral monomers, the average electrostatics may dominate the qualitative behavior of some properties. Among the reported observations is a coil-to-globule transition induced by lowering the temperature; the expanded flexible copolymer collapses to a globule of almost spherical shape. In this section we therefore study the coil-to-globule transition in the conditions of the simulation, which allow estimations of the contributions to the free energy of short-range attractive interactions using temperature as a variable.

Our model for the electrostatics of the coil-to-globule transition will be the conversion of a linear expanded polyelectrolye *P* to a sphere with uniform surface charge *S*. The tendency of the charged monomers in the simulation to reside on the surface of the globule justifies the choice of a surface-charged sphere. Moreover, our sphere is taken as large, in the sense defined in previous sections. For the polyelectrolyte we use the standard line-of-charges model, a straight line with point charges uniformly spaced along its length.[10,11] This model is more easily adapted to the bead model for the simulated copolymer than a thin cylinder with continuous surface charge and ambiguous radius. The simulations included only the macroion and its counterions with no additional electrolyte. We refer the reader back to part B of section II, which adapts the free energy to the counterions-only case.

The relevant temperature range in the simulations is such that the charge density of the expanded polyelectrolyte is below the threshold for counterion condensation. The large sphere, however, is supercritical, and does condense counterions. Therefore, the electrostatic component of the free energy of transition in units of k_BT is given by

$$\Delta g^{el} = \frac{N}{z}\left\{\left[\left(2-\frac{1}{\sigma_s'}\right)(-\ln \kappa_0\lambda_B) - 1 + \frac{1}{\sigma_s'}\right] + \frac{z\lambda_B}{b}\ln(1-e^{-\kappa_0 b})\right\} \quad (28)$$

where *N* is the number of charges common to polyelectrolyte and sphere, and *b* is the charge spacing in the linear assembly of *N* discrete charges modeling the polyelectrolyte. Notice that the polyelectrolyte part of this expression is linear in the charge density parameter $\xi = \lambda_B/b$, since the polyelectrolyte is taken as subcritical for counterion condensation, $z\xi < 1$, and that it does not require the condition $\kappa_0 b \ll 1$. In the intended application, we will have to check that $z\xi$ is indeed less than unity. The condition $\kappa_0\lambda_B \ll 1$ is assumed in the free energy component due to the sphere.

Quantities pertaining to the sphere are indicated by subscript *s*. The reduced surface charge density for the sphere $\sigma_s' = \sigma_s/\sigma_{s,crit}$ can be calculated from $\sigma_s = Ne/4\pi a_s^2$, and from eq 9 for $\sigma_{s,crit}$. In eq 9, however, the function $f_s(\kappa a_s)$, which equals $1/(1+\kappa a_s)$ for a large sphere according to eq 19, must be replaced by the function $\phi_s(\kappa_0 a_s)$ from eq 25, since only counterions are present. We then find that

$$\sigma_s' = -\frac{Nz\lambda_B\phi(\kappa_0 a_s)}{2a_s\ln(\kappa_0\lambda_B)} \quad (29)$$

with

$$\phi_s(\kappa_0 a_s) = \frac{(4+3\kappa_0 a_s)}{4(1+\kappa_0 a_s)^2} \quad (30)$$

For comparison with the simulation results, we should recast our quantities into the general dimensionless variables used by Khalatur et al. and Mologin et al. The authors measure lengths in terms of a unit that they call σ, which is the diameter of a monomer bead in their polymer chain of touching beads. Obviously, in the present context, we cannot use this notation, so we substitute the symbol δ for the unit of length. The average linear charge spacing *b* of the polyelectrolye chain is 2δ, since only half the beads in the simulated polymer are charged. There are 128 beads in each chain; so *N*, the number of monomers bearing unit charges, equals 64. The square of the Debye screening parameter κ_0^2 in the authors' units is $4\pi\lambda_B z^2\rho$, where ρ is the total number density of counterions, equal to $(1/2)(1.157\times10^{-3})/(z\delta^3)$ under the simulation conditions that give the sharpest coil-to-globule transition.[56]

The authors measured the radius of gyration of a single chain and in the range of temperatures where the chain is collapsed to a globule, which corresponds to our sphere *S*, they find a mean-square radius of gyration equal to about $5\delta^2$ for univalent counterions. Therefore, we take our sphere radius a_s to be equal to the square root, or 2.24δ.

Khalatur et al. and Mologin et al. also employ an energy unit ϵ, which determines the depth of their short-range Lennard-Jones potential. The temperature is measured by a dimensionless parameter that they call *T*, but which we, not having to consider dynamics in the present paper, prefer to designate by τ. With this notational change, their definition is $\tau = k_BT/\epsilon$, where *T* is the ordinary Kelvin temperature. We note that the Bjerrum length λ_B depends inversely on the temperature, and that the authors have set up their potentials such that $\lambda_B = \delta/\tau$. The linear charge density parameter ξ for the polyelectrolyte chain, that is, the ratio of λ_B to charge spacing *b*, is therefore equal to $(\delta/\tau)/2\delta$, or $1/2\tau$, so that the polyelectrolyte coil is subcritical for condensation of counterions of valence *z* if τ is greater than $z/2$, a temperature condition that is met by the calculations in this section. Conversion to the Khalatur et al. units in eqs 28−30 renders Δg^{el} a function of reduced temperature τ.

In addition to the contribution from electrostatics, hydrophobic interactions also participate in determining the total free energy. We note that Khalatur et al.[56] simulate the latter with a short-range attractive potential. It is therefore not the entropic hydrophobic free energy of real systems in water; it has a different temperature dependence. However, the attractive forces in the simulation do generate the characteristic core−shell structure of a hydrophobically driven globule, with charged groups on the outside and uncharged "hydrophobic" groups on the inside. From Figures 4 and 5 of Khalatur et al., which give total energy per particle (128 monomers plus 64 counterions = 192 particles), and, separately, the energy from Coulombic interactions, we can determine by subtraction the short-range

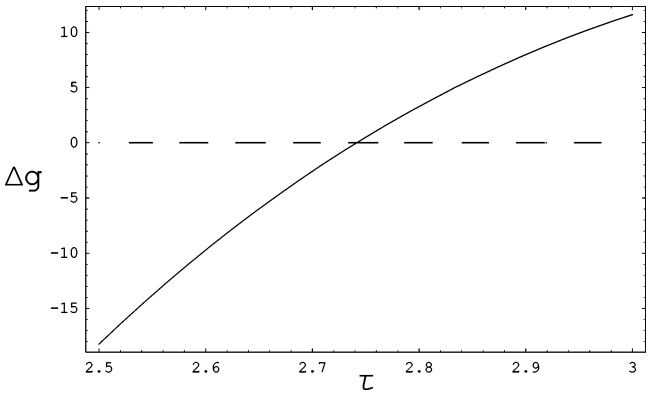

Figure 2. Coil-to-globule transition free energy in units of k_BT as a function of reduced temperature for univalent counterions.

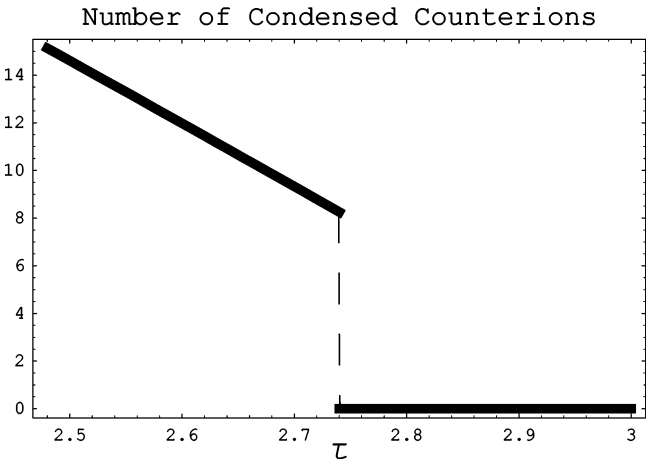

Figure 3. The number of condensed counterions jumps at the coil-to-globule transition temperature.

attractive energy of the globular form relative to the expanded coil at about -690ϵ, or, in units of k_BT, $-690/\tau$.

There is also a configurational free energy of entropic origin; when the flexible coil compacts to a highly constrained globule, there must be a significant decrease in entropy. However, the coil does not have a high charge density, and the hydrophobic interactions are still present within it. It is difficult to form a reliable estimate of the lost entropy, and our attempt to do so did not lead to consistent results. We have elected therefore to neglect this contribution.

At this point we may calculate the total free energy Δg as the sum of the electrostatic and hydrophobic contributions, and as indicated in Figure 2 for univalent counterions, we find a coil-to-globule transition induced by decreasing the temperature. The reduced temperature τ has the value 2.74 at the transition. If we think in terms of an ensemble of isolated chains, then the transition is quite sharp. Using Boltzmann factors, we calculate that at $\tau = 2.84$, only 1 of every 202 chains is spherical globular, while at $\tau = 2.64$, there are 804 globules for every expanded chain.

We have checked that our model of a large supercritical sphere for the globule is consistent with the simulation conditions. At the dilute concentration used, $\kappa\lambda_B = 0.019$ at the transition temperature and so qualifies as a small quantity. Moreover, $\sigma_s' = 1.15$, greater than the critical value unity. The value of the polyelectrolye charge parameter $\xi = 0.18$, so the polyelectrolye chain is indeed subcritical. In Figure 3 we show the jump in the number of condensed counterions as τ decreases through the transition from none on the polyelectrolyte chain to 8 on the spherical globule. The effective charge on the sphere, which carries 64 structural charges in the simulation, is equal to 56 at the transition temperature.

In the simulations a sharp coil-to-globule transition was observed at $\tau = 1.6$ for univalent counterions at the low concentration used in our calculations. At a higher concentration the transition was broadened, suggesting interchain interactions that we cannot model. For divalent and tetravalent counterions, simulations were reported only at the higher concentration where the transitions were very broad and merged with interchain aggregation.[57] Transition temperatures at the inflection points increased with valence of the counterion, reaching the value $\tau = 3.5$ for tetravalent counterions. Using the same low chain monomer concentration as above, we calculate transition temperatures 2.7, 4.9, and 8.7 for $z = 1$, 2, and 4, respectively. Our model captures the qualitative trend, but the critical temperatures are shifted up from the simulation results. We may note that the entropy of the degrees of freedom of the flexible chain, which we have neglected in our calculations, would favor stability of the coil and thus lower the transition temperatures.

V. Disintegration of a Charged Sphere

In a kinetic computer experiment with two of the copolymeric chains described in the previous section, Khalatur et al.[56] prepared an equilibrated initial state at the reduced temperature $\tau = 1$ with the Coulomb interactions turned off. In these conditions the two chains associated due to their hydrophobic interactions, forming a two-chain globule with nearly spherical shape. The repulsive electrostatic interactions were then turned back on, and the evolution of the structure at constant τ was followed in time. The two chains were observed in a series of snapshots to disintegrate into two identical single-chain globules. The process is fast, suggesting only a small kinetic barrier, if any. The authors point to an early laboratory experiment of Lord Kelvin in which electrification of a water droplet results in elongation and rupture of the droplet into two droplets of equal size each with the same electrical charge.[51,56]

Khalatur et al. performed this experiment to show that their single-chain globule is a robustly stable structure. As discussed in section IV, the single-chain globule in their simulations results from the folding of an expanded coil when the temperature is lowered past $\tau = 1.6$, but there is no tendency toward multichain aggregation until the temperature is lowered by about a factor of 4 from this critical value. An attempt to force aggregation to a two-chain globule at $\tau = 1$ by the method just described results in rapid disintegration by electrostatic repulsion back to single-chain globules.

As an application of the free energy calculations in the present paper, we try to model the disintegration of a two-chain globule. To that end, we consider the disintegration process $S_2 \rightarrow 2S_1$, where S_2 is a charged sphere of radius a_2, and S_1 is a charged sphere of smaller radius a_1. The numerical subscripts suggest models for the two-chain and single-chain globules. The sphere S in section IV on the transition from a single-chain coil to a single-chain globule is the same as the sphere S_1 in this section. We will assume that the packing in S_2 is the same as in S_1 with preservation of the total volume, $(4/3)\pi a_2^3 = 2(4/3)\pi a_1^3$, so that $a_2 = 2^{1/3}a_1$.

We will consider both the electrostatic and hydrophobic free energies in this disintegration process, and we begin with the former. We assume the number of surface charges to be preserved. If sphere S_2 has $2N$ elementary surface charges e, then S_1 has N. The surface charge density σ_2 of S_2 equals $2Ne/4\pi a_2^2$. Then for sphere S_1, $\sigma_1 = N/4\pi a_1^2 = 2^{-1/3}\sigma_2$.

We will assume that both spheres S_2 and S_1 are large, in the sense we have discussed. We assume as well that the surface

charge densities of both spheres are greater than their respective critical values. These assumptions will be validated by the calculations. The critical value $\sigma_{2,\mathrm{crit}}$ for sphere S_2 is given by eq 9 with ℓ equal to the Bjerrum length λ_B and, since the only small ions in the system are the counterions of the spheres, with κ replaced by κ_0 from eq 26, and $f(\kappa a)$ from eq 2 replaced by $\phi(\kappa_0 a)$ from eq 25. An analogous expression holds for $\sigma_{1,\mathrm{crit}}$, which is easily demonstrated to be related to $\sigma_{2,\mathrm{crit}}$

$$\sigma_{1,\mathrm{crit}} = \frac{2^{1/3}\phi(\kappa_0 a_2)}{\phi(2^{-1/3}\kappa_0 a_2)}\,\sigma_{2,\mathrm{crit}} \tag{31}$$

It is equally straightforward to find the relation between σ_1' and σ_2', recalling the definition of σ' as $\sigma/\sigma_{\mathrm{crit}}$

$$\sigma_1' = 2^{-2/3}\,\frac{\phi(2^{-1/3}\kappa_0 a_2)}{\phi(\kappa_0 a_2)}\,\sigma_2' \tag{32}$$

Finally, the relation between the effective number of charges on the spheres after counterion condensation is

$$N_{1,\mathrm{eff}} = \frac{2^{-1/3}\phi(\kappa_0 a_2)}{\phi(2^{-1/3}\kappa_0 a_2)}\,N_{2,eff} \tag{33}$$

With these various connections between spheres S_2 and S_1, we can actually write a neat formula for $\Delta g^{el} = 2g^{el}(S_1) - g^{el}(S_2)$, the electrostatic free energy in units of k_BT for the disintegration $S_2 \rightarrow 2S_1$

$$\Delta g^{el} = \frac{1}{z}\,N_{2,\mathrm{eff}}\left[2^{2/3}\,\frac{\phi(\kappa_0 a_2)}{\phi(2^{-1/3}\kappa_0 a_2)} - 1\right][\ln(\kappa_0\lambda_B) + 1] \tag{34}$$

where

$$N_{2,\mathrm{eff}} = \frac{2a_2}{z\lambda_B\phi(\kappa_0 a_2)}\,(-\ln(\kappa_0\lambda_B)) \tag{35}$$

Notice that since $\kappa_0\lambda_B$ is small, Δg^{el} is negative, signifying that uncompensated electrostatic repulsion would drive the disintegration of sphere S_2 into two smaller spheres S_1 each with less charge.

As in section IV, we also use here the unit quantities employed by Khalatur et al. As explained in section IV, the radius of sphere S_1 (denoted in that section by a_s) has a given value $a_1 = \sqrt{5}\delta = 2.24\delta$, so that the value of the radius of the 2-sphere that appears in our formula for Δg^{el} becomes $a_2 = 2^{1/3}a_1 = 2.82\delta$. The Debye screening parameter κ_0 is specified in the simulation to have the same value as given in section IV with the exception that the number density ρ of counterions is twice that in section IV, since the simulation involves two chains instead of one. Again as in section IV, the Bjerrum length equals δ/τ, where τ is the reduced temperature. The unit length δ then cancels in the expression for Δg^{el}, which becomes a function of the single environmental variable τ.

We have checked that in the range of relevant temperatures, both σ_1' and σ_2' exceed unity, so that both the 1-sphere and the 2-sphere are supercritical with respect to counterion condensation as assumed in the development above. Moreover, the quantity $\kappa_0\lambda_B$ is small in the range, while both $\kappa_0 a_1$ and $\kappa_0 a_2$ are larger, thus justifying use of the large-sphere model (for example, at $\tau = 2$ these three quantities in respective order equal 0.04, 0.19, and 0.24).

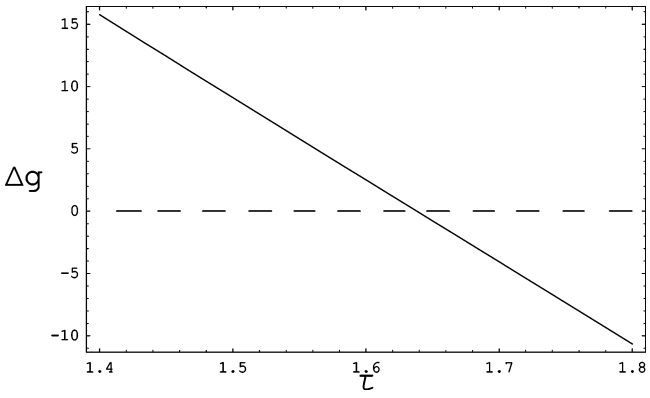

Figure 4. Free energy change in units of k_BT for the disintegration of a 2-sphere into two unit spheres as a function of reduced temperature. The counterions are univalent.

Concerning the hydrophobic component of the free energy, we recall from section IV that the short-range attractive ("hydrophobic") energy of S_1 can be estimated from the simulation itself as about -690ϵ, where ϵ is the unit of energy. More precisely, this value is the energy change when a globule with surface area (in our spherical model) $4\pi a_1^2$ is formed from an expanded random coil that is more or less fully exposed to solvent. The initial (expanded coil) surface area is about equal to $128(4\pi)(1/4)\delta^2$, since the chain consists of 128 monomer beads of radius $(1/2)\delta$. Since $a_1^2 = 5\delta^2$ (see above), the change of exposed surface area in the coil−globule transition is then $-27(4\pi)\delta^2$. Dividing the hydrophobic energy change -690ϵ by the surface area change, we get a conversion factor, (Δ energy)/(Δ surface area), equal to $(26/4\pi)(\epsilon/\delta^2)$.

The increase of exposed surface area in the disintegration process $S_2 \rightarrow 2S_1$ equals $4\pi(2a_1^2 - a_2^2)$, or, $4\pi(2 - 2^{2/3})a_1^2$, or, $4\pi(2 - 2^{2/3})5\delta^2$. Using the conversion factor from the previous paragraph, we find that the corresponding hydrophobic energy change is 54ϵ, or, since $\epsilon = k_BT/\tau$

$$\Delta g^{hyd} = 54/\tau \tag{36}$$

for a rough estimate of the "hydrophobic" free energy change in units of k_BT as adapted to our model.

In Figure 4, we plot the total free energy change $\Delta g = \Delta g^{el} + \Delta g^{hyd}$ in units of k_BT for the disintegration process $S_2 \rightarrow 2S_1$ with univalent counterions. We see that the 2-sphere S_2 becomes unstable when $\tau > 1.64$. Thus, we are able to model the simulated disintegration experiment of Khalatur et al., but only by an upward shift in the relevant temperatures. Whereas the authors found spontaneous disintegration at $\tau = 1$, we find corresponding temperatures only in the range $1.6 < \tau < 3.0$, the upper bound being the temperature at which S_1 opens to a coil (as in section IV, but at the concentration used in this section). In our model, a two-chain globule is actually stable against disintegration at $\tau = 1$ (Figure 4).

Khalatur et al. engaged in an extensive analysis of counterion condensation in their system, as measured by several criteria, including direct visualization, all yielding similar results. They interpret the stability of the single-chain globule as the result of partial counterion condensation, which yields an effective charge on the globule less than its bare charge, but one that is large enough to prevent aggregation over a wide temperature range. Our model is consistent with this interpretation. We may look, for example, at the temperature $\tau = 2$, where we find that S_1 is stable against opening to a coil (section IV), but where S_2 spontaneously disintegrates into two spheres S_1. At this temperature we calculate the effective charge on S_1 as 35, reduced

from its bare charge 64 by condensation of 29 univalent counterions. Similarly, the effective charge on S_2 is 46, reduced by condensation of 82 univalent counterions from its bare charge 128. Thus, even though the condensation of 24 counterions (82 minus twice 29) accompanies the formation of S_2 from two spheres S_1, the effective charge on the former is still great enough to cause it to spontaneously disintegrate, emitting, or releasing, the extra 24 counterions as part of the disintegration process.

VI. Growth of Charged Spheres

Figure 4 indicates two distinct kinds of behavior of the 2-sphere S_2. At high temperatures, $\tau > 1.6$ under the conditions specified, it spontaneously disintegrates into two 1-spheres. At lower temperatures, however, it is stable against disintegration, and indeed, for $\tau < 1.6$, it is the reverse process that has a negative free energy; that is, two 1-spheres S_1 spontaneously fuse to form the larger sphere S_2. The aggregation process observed by Khalatur et al.[56] at very low temperatures is complex. With univalent counterions two charged single-chain globules do not fuse into a spherical shape. Instead, two intact single-chain globules approach and almost touch, forming an elongated dimer (a few trimers are also formed). The authors comment on the remarkable stability of the intact single-chain globule against a tendency toward large-scale aggregation and precipitation. An attempt to describe such a process with a simple model would require calculation of the interaction of two charged spheres as a function of distance between them, but we are not able to perform this analysis at present. In the presence of multivalent counterions Mologin et al.[57] do observe spherical aggregates formed from interpenetration of several chains, but charged monomers and counterions are found in the interiors of these objects, rendering our model of impenetrable surface-charged spheres perhaps overly idealized. In this section we therefore adopt a restricted objective, which is to show how a simple model that counters repulsive electrostatics with short-range attractions can lead either to noncooperative limited growth or to cooperative macroscopic precipitation, depending on the pathway for aggregation.

We begin by giving a precise definition of an n-sphere S_n. Then we assume that an n-sphere and an m-sphere can fuse into an $(m + n)$-sphere, and in fact we will find that this process is spontaneous at low temperatures. We will analyze two different modes of growth by this type of fusion. In the first, a 1-sphere fuses with an n-sphere to form an $(n + 1)$-sphere, which then fuses with another 1-sphere to form an $(n + 2)$-sphere, and the process continues. In the second, two n-spheres fuse to form a $2n$-sphere, two of the $2n$-spheres thus formed fuse to form a $4n$-sphere, and the process continues. We find that the first mode of growth is noncooperative with many intermediates present. It would not lead to large-scale aggregation and precipitation. In contrast, the second model is cooperative and would lead to macroscopic precipitation.

Supposing that an n-sphere S_n has the same volume as the total volume of n unit spheres S_1, we have for its radius, $a_n = n^{1/3}a_1$. Moreover, if the number of bare unit charges on the surface of S_n is n times the number of charges N on S_1, the relation between the bare surface charge densities of S_n and S_1 also works out to be $\sigma_n = n^{1/3}\sigma_1$. The reduced charge density of S_n (ratio of σ_n to $\sigma_{n,\mathrm{crit}}$) is

$$\sigma_n' = \sigma_1' n^{2/3} \frac{\phi(n^{1/3}\kappa_0 a_1)}{\phi(\kappa_0 a_1)} \tag{37}$$

where for the unit sphere S_1

$$\sigma_1' = -\frac{Nz\lambda_B \phi(\kappa_0 a_1)}{2a_1 \ln(\kappa_0 \lambda_B)} \tag{38}$$

a relation that is the same as eq 29 but with the notation of the present section.

We can write a general fusion process

$$S_n + S_m \rightarrow S_{n+m} \tag{39}$$

In units of k_BT the electrostatic free energy for this process can be obtained from the large-sphere model using eq 15

$$\Delta g^{el} = \frac{N}{z}[\ln(\kappa_0 \lambda_B) + 1]\left[\frac{n+m}{\sigma_{n+m}'} - \frac{n}{\sigma_n'} - \frac{m}{\sigma_m'}\right] \tag{40}$$

In the calculations below, we take the number density of counterions equal to $1.678 \times 10^{-2}/(z\delta^3)$, corresponding to the multichain simulations of Khalatur et al.[56] Then the Debye screening parameter κ_0 is calculated as in section IV, $\lambda_B = \delta/\tau$ with τ the reduced temperature as explained in that section, and $a_1 = \sqrt{5}\delta$, again as in sections IV and V. The number of bare charges on the unit sphere is $N = 64$, and our calculations are for univalent counterions, $z = 1$. The calculations indicate that Δg^{el} is a positive quantity, unfavorable for the growth of spheres by fusion.

For the "hydrophobic" free energy change we need the decrease of exposed surface area $\Delta A = 4\pi(a_{n+m}^2 - a_n^2 - a_m^2)$ when S_n and S_m fuse to form the larger sphere S_{n+m}. Since the radii of all of these spheres are related to a_1 as discussed above, we find, $\Delta A = 4\pi a_1^2[(n + m)^{2/3} - n^{2/3} - m^{2/3})]$. Using the conversion factor calculated in section V, we obtain for the hydrophobic free energy change Δg^{hyd} in units of k_BT

$$\Delta g^{hyd} = \frac{130}{\tau}[(n + m)^{2/3} - n^{2/3} - m^{2/3}] \tag{41}$$

The negative values of Δg^{hyd} favor fusion.

As indicated in the introduction to this section, we will examine two modes of sphere growth. In the first, which we call *growth by unitary fusion*, the sequence is $S_1 + S_1 \rightarrow S_2$, $S_2 + S_1 \rightarrow S_3$, ..., $S_n + S_1 \rightarrow S_{n+1}$, ..., in other words, a sphere grows by absorbing a unit sphere. The sequence for the second mode, designated *growth by twin fusion*, is $2S_1 \rightarrow S_2$, $2S_2 \rightarrow S_4$, $2S_4 \rightarrow S_8$, ..., $2S_{2^j} \rightarrow S_{2^{j+1}}$, ...; that is, a growing sphere fuses with another of equal size to form one with twice the volume.

Limiting values of the free energies for both modes of growth can be calculated. For example, we find for unitary fusion at the fixed temperature $\tau = 2$ that at the limit $n \rightarrow \infty$, $\Delta g^{el} = +26$, while $\Delta g^{hyd} = -65$, the net value -39 favoring further growth. In other words, for very large n, the free energy of the nth growth step in unitary fusion, $S_n + S_1 \rightarrow S_{n+1}$, approaches the finite limit $-39k_BT$. The significance is perhaps most easily seen if we invoke an obvious mathematical fact, that in an infinite sequence of numbers tending to a finite limit, the difference between the nth number and the $(n - 1)$th must become progressively smaller. In the case at hand, let Δg_n be the net free energy of the nth growth step (electrostatic plus hydrophobic). Then $\Delta g_n - \Delta g_{n-1}$ must tend to zero if $n \rightarrow \infty$, and indeed, we have verified this result by direct calculation (see below). The physical meaning emerges clearly. For large n, the free energy of fusing a unit sphere with an n-sphere is almost the same as for fusion of a unit sphere with an $(n -$

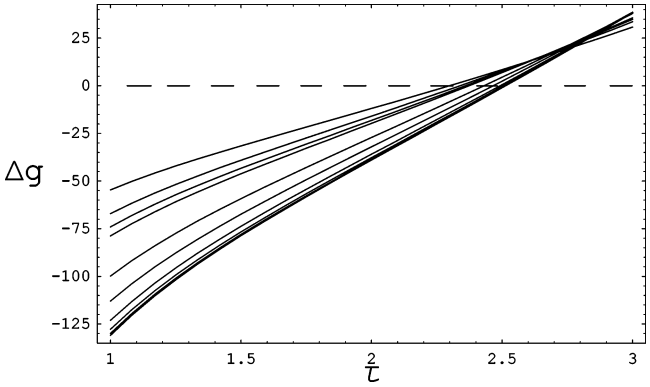

Figure 5. Illustration of noncooperative unitary fusion. Each curve is at a fixed value of n and indicates as a function of reduced temperature the free energy change (units of k_BT, univalent counterions) for the process of fusing a unit sphere into an n-sphere to form an $(n + 1)$-sphere. The range of n is from 1 to 10^6, top to bottom.

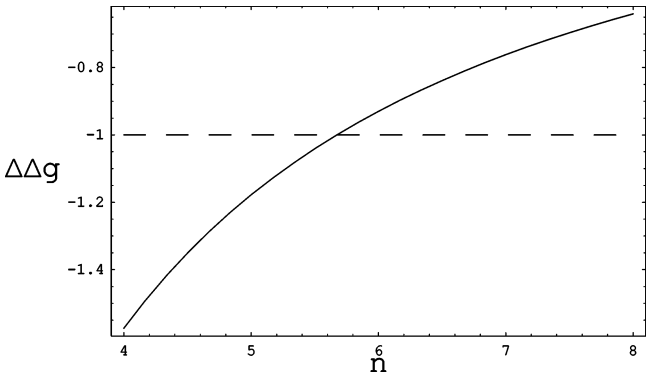

Figure 6. Plot of the free energy change (units of k_BT, univalent counterions) for fusing a unit sphere with an n-sphere, relative to the free energy change for fusing a unit sphere with an $(n - 1)$-sphere, as a function of n. The plot shows that this relative free energy becomes less than k_BT when n exceeds 6.

1)-sphere. Growth by unitary fusion is a noncooperative process. Large-scale aggregation leading to macroscopic precipitation does not occur. There always remain many spheres of intermediate sizes.

We illustrate this analysis of unitary fusion in Figures 5 and 6. Figure 5 shows the temperature dependence of the free energy of each member of a sequence of growth steps up to a large value of n. For $\tau = 2$ (and for smaller values) the growth steps are increasingly favorable, but the approach to a limit is obvious. Figure 6 is a plot with the temperature fixed at $\tau = 2$. The function plotted is $\Delta\Delta g(n) = \Delta g(n) - \Delta g(n - 1)$, namely, the difference between the free energy of the nth step and the $(n - 1)$st. The plot shows that the growth of an n-sphere by unitary fusion is favored by a free energy less than k_BT if n is greater than 6. Thermal disruption, therefore, will prevent macroscopic aggregation. The same conclusion is reached if we notice that $\Delta\Delta g(n)$ is the free energy change for the process, $2S_n \rightarrow S_{n-1} + S_{n+1}$, in which an n-sphere emits a unit sphere that is absorbed by another n-sphere. Figure 6 then shows that this process is about as likely to go backward as forward if $n \geq 6$, shrinking an $(n + 1)$-sphere back to an n-sphere. Still another way to look at growth of spheres by unitary fusion is that it occurs in effectively high-temperature conditions. For sphere sizes greater than modest ones, all spheres regardless of size are present in about equal populations.

Twin fusion behaves in a radically different manner. The electrostatic free energy Δg_j^{el} for the process $2S_{2^j} \rightarrow S_{2^{j+1}}$ diverges to $+\infty$ when $j \rightarrow \infty$, but the hydrophobic component

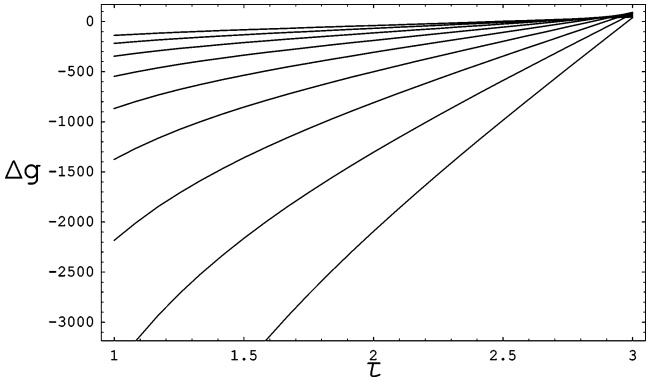

Figure 7. Illustration of cooperative twin fusion. Each curve is at a fixed value of the index j and indicates as a function of reduced temperature the free energy change (units of k_BT, univalent counterions) for the process of fusing two n-spheres to form a $2n$-sphere, $n = 2^j$. The range of j is from 0 to 10, top to bottom.

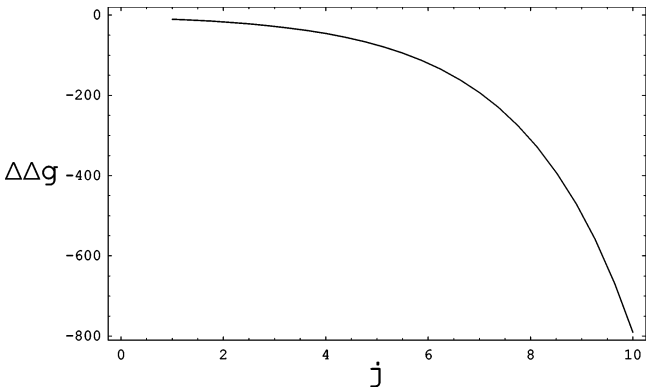

Figure 8. Plot of the free energy change (units of k_BT, univalent counterions) for fusing two n-spheres, $n = 2^j$, into a $2n$-sphere, relative to the free energy change for fusing two $(n - 1)$-spheres, as a function of j.

Δg_j^{hyd} diverges to $-\infty$ in such a way that the overall free energy Δg_j becomes negatively infinite. The infinities are such that growth is cooperative. For large j the negative free energy of the j-th growth step becomes infinitely greater than for the previous step, $\Delta\Delta g_j \rightarrow -\infty$. These results of direct calculation are illustrated numerically in Figures 7 and 8, which may be contrasted respectively with Figures 5 and 6 for unitary fusion.

At the outset of this section we were cautious in noting that the results to be obtained could not be compared directly with the simulation data of Khalatur et al.[56] showing stability of single-chain globules against large-scale aggregation even at very low temperatures. Nonetheless, we believe our results may be related. It is difficult to conceive of a mechanistic pathway for growth by twin fusion in their system, much easier to imagine growth by progressive absorption of single chains, leading as we have seen to aggregates of limited size. Indeed, the latter mechanism predicts arrest of growth at a small aggregate number of about 6, and the model of surface-charged spheres with no charged groups or monovalent counterions trapped in the interiors is at least qualitatively reasonable for such a small aggregate.

Acknowledgment. The author gratefully acknowledges private correspondence with Pavel Khalatur and Alexei Khokhlov.

References and Notes

(1) Manning, G. S. *Acc. Chem. Res.* **1979**, *12*, 443.
(2) Manning, G. S. *Ber. Bunsen-Ges. Phys. Chem.* **1996**, *100*, 909.

(3) Whitlock, L. R. In *New Directions in Electrophoretic Methods*; Jorgenson, J. W., Phillips, M., Eds.; ACS Symposium Series 335; American Chemical Society: Washington, DC, 1987; p 222.
(4) Shaaban, A. H.; Ander, P. *Polym. Prepr.* **1993**, *34*, 970.
(5) Hoagland, D. A.; Smisek, D. L.; Chen, D. Y. *Electrophoresis* **1996**, *17*, 1151.
(6) Popov, A.; Hoagland, D. A. *J. Polym. Sci., Part B: Polym. Phys.* **2004**, *42*, 3616.
(7) Gao, J. Y.; Dubin, P. L.; Sato, T.; Morishima, Y. *J. Chromatogr. A* **1997**, *766*, 233.
(8) Zana, R.; Tondre, C.; Rinaudo, M.; Milas, M. *J. Chim. Phys.* **1971**, *68*, 1258.
(9) Keyser, U. F.; Koeleman, B. N.; Van Dorp, S.; Krapf, D.; Smeets, R. M. M.; Lemay, S. G.; Dekker, N. H.; Dekker, C. *Nat. Phys.* **2006**, *2*, 473.
(10) Manning, G. S. *Q. Rev. Biophys.* **1978**, *11*, 179.
(11) Manning, G. S. *Biophys. Chem.* **2002**, *101*−*102*, 461.
(12) Savelyev, A.; Papoian, G. A. *J. Am. Chem. Soc.* **2006**, *128*, 14506.
(13) Lampert, M. A. *Biopolymers* **1982**, *21*, 159.
(14) Ramanathan, G. V.; Woodbury, C. P. *J. Chem. Phys.* **1982**, *77*, 4133.
(15) Ramanathan, G. V. *J. Chem. Phys.* **1983**, *78*, 3223.
(16) Zimm, B. H.; Le Bret, M. *J. Biomol. Struct. Dyn.* **1983**, *1*, 461.
(17) Manning, G. S. *Physica A* **1996**, *231*, 236.
(18) Mohanty, U.; Ninham, B. W.; Oppenheim, I. *Proc. Natl. Acad. Sci. U.S.A.* **1996**, *93*, 4342.
(19) Rouzina, I.; Bloomfield, V. A. *J. Phys. Chem.* **1996**, *100*, 4292.
(20) Tracy, C. A.; Widom, H. *Physica A* **1997**, *244*, 402.
(21) Young, M. A.; Jayaram, B.; Beveridge, D. L. *J. Am. Chem. Soc.* **1997**, *119*, 59.
(22) Levin, Y.; Barbosa, M. C. *J. Phys. II* **1997**, *7*, 37.
(23) Winkler, R. G.; Gold, M.; Reineker, P. *Phys. Rev. Lett.* **1998**, *80*, 3731.
(24) Feig, M.; Pettitt, B. M. *Biophys. J.* **1999**, *77*, 1769.
(25) Qian, H.; Schellman, J. A. *J. Phys. Chem. B* **2000**, *104*, 11528.
(26) Deserno, M.; Holm, C.; May, S. *Macromolecules* **2000**, *33*, 199.
(27) Netz, R. R.; Orland, H. *Eur. Phys. J. E* **2003**, *11*, 301.
(28) Mohanty, U.; Spasic, A.; Kim, H. D.; Chu, S. *J. Phys. Chem. B* **2005**, *109*, 21369.
(29) Naji, A.; Netz, R. R. *Phys. Rev. E* **2006**, *73*, 056105.
(30) Trizac, E.; Tëllez, G. *Phys. Rev. Lett.* **2006**, *96*, 038302.
(31) Long, H.; Kudlay, A.; Schatz, G. C. *J. Phys. Chem. B* **2006**, *110*, 2918.
(32) Manning, G. S. *J. Chem. Phys.* **1969**, *51*, 3249.
(33) Stevens, M. J.; Plimpton, S. J. *Eur. Phys. J. B* **1998**, *2*, 341.
(34) Marky, N. L.; Manning, G. S. *J. Am. Chem. Soc.* **2000**, *122*, 6057.
(35) Manning, G. S. *J. Am. Chem. Soc.* **2003**, *125*, 15087.
(36) Manning, G. S. *Biopolymers* **2003**, *69*, 137.
(37) Manning, G. S. *Biophys. J.* **2006**, *91*, 1.
(38) Schulz, S. F.; Sticher, H. *Prog. Colloid Poly. Sci.* **1994**, *97*, 85.
(39) Martin-Molina, A.; Quesada-Perez, M.; Galisteo-Gonzalez, T.; Hidalgo-Alvarez, R. *J. Phys. Chem. B* **2002**, *106*, 6881.
(40) Huang, Q. R.; Dubin, P. L.; Moorefield, C. N.; Newkome, G. R. *J. Phys. Chem. B* **2000**, *104*, 898.
(41) Welch, C. F.; Hoagland, D. A. *Langmuir* **2003**, *19*, 1082.
(42) Guo, X.; Kirton, G. F.; Dubin, P. L. *J. Phys. Chem. B* **2006**, *110*, 20815.
(43) Pandit, S. A.; Berkowitz, M. L. *Biophys. J.* **2002**, *82*, 1818.
(44) Romsted, L. S. *Langmuir* **2007**, *23*, 414.
(45) Belloni, L.; Drifford, M.; Turq, P. *Chem. Phys.* **1984**, *83*, 147.
(46) Alexander, S.; Chaikin, P. M.; Grant, P.; Morales, G. J.; Pincus, P. *J. Chem. Phys.* **1984**, *80*, 5776.
(47) Ramanathan, G. V. *J. Chem. Phys.* **1988**, *88*, 3887.
(48) Belloni, L. *Colloids Surf. A* **1998**, *140*, 227.
(49) Lau, A. W. C.; Lukatsky, D. B.; Pincus, P.; Safran, S. A. *Phys. Rev. E* **2002**, *65*, 051502.
(50) Manning, G. S. *J. Phys. Chem. B* **2007**, *111*, 8554.
(51) Reviewed, in Khokhlov, A. R.; Khalatur, P. G. *Curr. Opin. Colloid Interface Sci.* **2005**, *10*, 22.
(52) Ha, B.-Y.; Liu, A. J. *Europhys. Lett.* **1999**, *46*, 624.
(53) Potemkin, I. I.; Vasilevskaya, V. V.; Khokhlov, A. R. *J. Chem. Phys.* **1999**, *111*, 2809.
(54) Ray, J.; Manning, G. S. *Macromolecules* **2000**, *33*, 2901.
(55) Verwey, E. J. W.; Overbeek, J. Th. G. *Theory of the Stability of Lyophobic Colloids*; Dover: New York, 1999.
(56) Khalatur, P. G.; Khokhlov, A. R.; Mologin, D. A.; Reineker, P. *J. Chem. Phys.* **2003**, *119*, 1232.
(57) Mologin, D. A.; Khalatur, P. G.; Khokhlov, A. R.; Reineker, P. *New J. Phys.* **2004**, *6*, 133.

MA071457X